THE JOURNAL OF PHYSICAL CHEMISTRY C

Article

Cite This: J. Phys. Chem. C 2018, 122, 23271−23279

pubs.acs.org/JPCC

Benchmarking the Electronic Processes at the Planar Organic Heterojunction Solar Cells

Dan Liraz, Himanshu Shekhar, Lior Tzabari, and Nir Tessler*

Microelecronic & Nanoelectronic Centers, Electrical Engineering Department, Technion Israel Institute of Technology, Haifa 32000, Israel

Supporting Information

ABSTRACT: While there exist several models for organic heterojunction solar cells, there is still a need for one that is both general and flexible to compare the relative importance of the plethora of potential processes. We describe a modeling framework that allows one to compare the relative importance of different physical processes, taking place in organic heterojunction-based photocell, on equal footing. The framework is based on rate equations, making it easy to modify and include processes not explicitly introduced here. To apply this approach, we fabricated several heterojunction devices. Applying this new methodology for a given device structure, we used a single set of parameters to fit four different experiments extending over a wide range of applied voltage and 5 orders of magnitude of light intensity. As an example, and as a result of the self-consistency of the joint modeling and experiment, we find that the charge generation and charge recombination do not take place through the same set of interface states (i.e., much can be gained through material and morphology design). In addition, by including the detailed balance between charge transfer excitons' generation and dissociation, we found that the bimolecular Langevin recombination through the charge transfer excitons is not strong enough to account for the losses in the photocells.

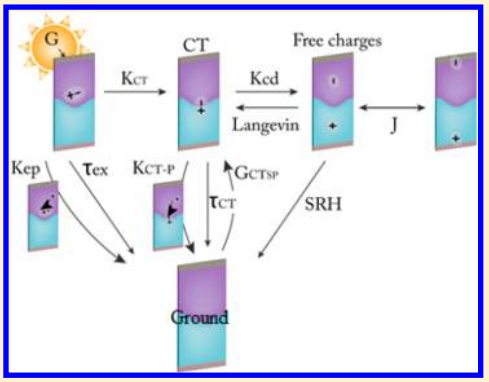

1. INTRODUCTION

Thin film solar cells offer aid to reduce the cost of solar energy production by exploiting cheap materials combined with simple processing techniques for installation of large area, mechanically rugged modules. To date, several material systems have achieved the commercial target of >10% power conversion efficiency (PCE), at least in lab-tested cells.[1] Current technologies are based mainly on the "traditional" semiconductors, Si and GaAs, where single junction efficiencies approach their theoretical values.[2] Organic photovoltaics (OPV) have emerged as well-performing, solution-processed solar cells; however, their current best performances (∼12%) are significantly lower than the theoretical predictions (20−24%).[3,4] The "rising star" of photovoltaics−organic−inorganic halide perovskite solar cells (PSC) very rapidly approached high performances (22%), but currently lack the stability and reproducibility required for a viable technology.[5] A seminal limiting factor in almost all thin film technologies is that, while they deliver sufficient short-circuit currents, their open-circuit voltages (V_{OC}) are low.

Focusing on the OPV technology, it is clear that by improving the V_{OC} the devices would prove to be commercially viable. It is also clear that much of what matters, using today's materials, is determined by the interfaces, be them the donor−acceptor interface or the contact's interface. However, what physical process is limiting the contribution of the interface to the solar cell performance is not clear or at least is not agreed upon by different groups. If one could pinpoint the "problematic" processes and quantify their relative importance to the solar cell efficiency, then one could proceed with judicious material and interface design so as to approach the theoretical predictions of ∼20%.[3,4] It is our understanding that the lack of consensus is partly due to many characterization methods not being carried out under the solar cell's operating conditions. The other part is a lack of a common basis for the interpretation of experimental data in terms of relevant physical processes. We present a robust and flexible model and apply it to heterojunction solar cells measured under relevant operating conditions. We show how the model can assist in quantifying the relative contribution of processes and provide a solid physical framework. Moreover, one could change and modify the model to test additional processes that are considered as potential contributors to the cell's efficiency. In this contribution, we present the model for a planar heterojunction, which may seem like a setback as compared to some bulk-heterojunction devices. However, even if this was true, we consider the establishment of a common framework in planar heterojunction as an essential step toward doing the same for bulk-heterojunctions.[6]

Received: July 4, 2018
Revised: September 13, 2018
Published: September 25, 2018

DOI: 10.1021/acs.jpcc.8b06404
J. Phys. Chem. C 2018, 122, 23271−23279

2. MODELING FRAMEWORK

Before presenting the model equations, we describe the essence of it. Figure 1a shows a schematic description of planar

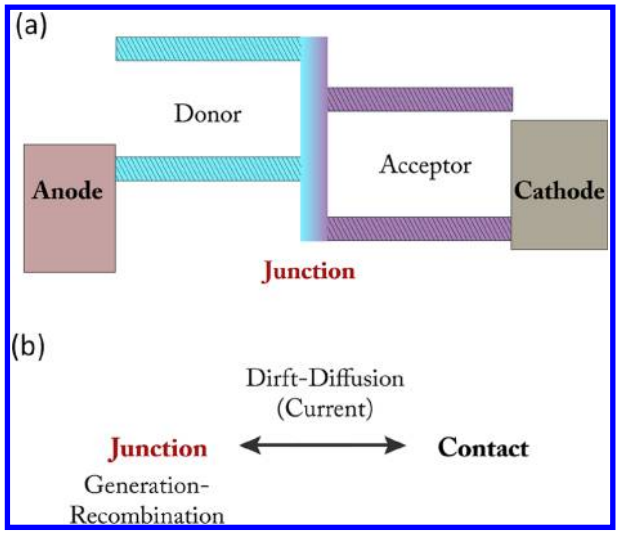

Figure 1. (a) Schematic description of a planar heterojunction organic photocell. (b) Illustration of the modeling concept used here.

organic heterostructure, which is the focus of this Article. The active part is a bilayer structure of donor and acceptor materials stacked on top of each other. Because these are excitonic semiconductors, it is accepted that, although light may be absorbed in the two films, the generation and recombination of charges take place only at the junction, or interface, between the two materials. The connection with an external circuit is through the cathode and anode, which are at the acceptor and donor sides, respectively.

There has been extensive modeling effort toward the understanding of bulk heterojunction solar cells,[7−21] while there are significantly fewer reports regarding the planar heterostructure device.[22−25] However, the planar heterostructure better lends itself for the understanding of the underlying physics. In the planar heterostructure, one can almost intuitively separate between charge-transport and the generation-recombination processes (see Figure 1b), thus allowing for critical examination of the processes taking place at the heterojunction. To some extent, our modeling approach is similar to ref 22 with the interface processes being those considered in refs 26 and 27. However, the present model covers a significantly broader set of operating conditions and thus a wide range of experiments. We found it was essential to be able to fit a range of measurements to choose from the various processes suggested in the literature.

Figure 2a shows the 3D device structure and illustrates the process block to be used in our modular framework. The notion is that one can add processes (physics) and that in the general case the generation of current evolves from one block to the next while allowing for losses (to the ground state). Figure 2b describes the physical processes being considered here and their mutual interactions as a flow-diagram. Starting from the left, the processes that positively contribute to the current generation are exciton (ex) generation (G) in the donor or acceptor layer, transfer or conversion of excitons (K_{CT}) to the charge transfer (CT) states, dissociation (K_{cd})[28] from the CT states into free electron (n) and hole (p), drift,

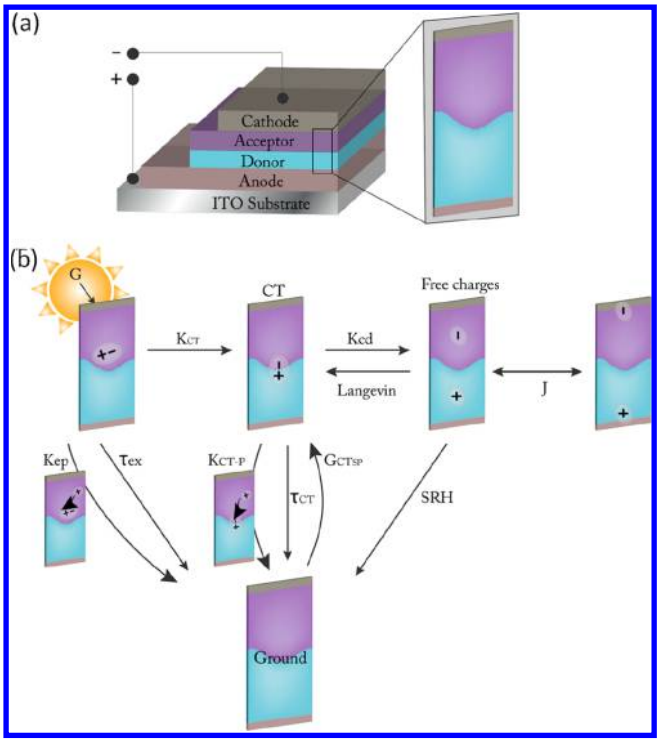

Figure 2. (a) 3D device structure and illustration of a process block to be used in (b). (b) Flow diagram of the processes accounted for in the basic model used here.

and diffusion (J) of charges to the contacts. For each of the excitons, CTs, and charges, there are competing mechanisms that reduce the cell's efficiency. For the excitons and CTs, there is the decay rate ($1/\tau$) that is a combination of radiative and nonradiative decay. An additional decay rate, which is probable for organic cells, is the quenching of excitons (K_{ep}) or CTs (K_{CTp}) by polarons,[16,29] either electrons or holes. The free electrons and holes, residing on their respective sides of the junction, may recombine[30] back into CTs ($\mathcal{L}$Langevin) or recombine through deeper lying states (SRH).[31,32] As the involved band-gaps are relatively large, it is common to neglect the thermal generation of excitons or CTs. However, as will be discussed below, the self-consistency of the model required the inclusion of spontaneous generation for the CTs (G_{CTsp}).

2.1. Equations of the Basic Model. In the model's equations, we consider explicitly only three populations: excitons, charge transfer excitons, and free polarons. The deep states at the junction are implicitly included in the expression for the SRH recombination. We first consider only the junction, and the three rate equations describing the processes at the junction are

$$\frac{dn_{ex}}{dt} = G - \frac{1}{\tau_{ex}} n_{ex} - K_{ep} p n_{ex} - K_{CT} n_{ex} = 0 \quad (1)$$

where n_{ex} is the exciton density in the absorbing layer, G is the exciton generation rate through light absorption, p is the free polaron density at the vicinity of the junction, K_{ep} is the positive polaron-exciton annihilation rate, τ_{ex} is the exciton lifetime, and K_{CT} is the rate of exciton transfer into CT excitons. The equation describing the evolution of CT excitons is

DOI: 10.1021/acs.jpcc.8b06404
J. Phys. Chem. C 2018, 122, 23271−23279

$$\frac{dn_{CT}}{dt} = K_{CT}n_{ex} - \frac{1}{\tau_{CT}}n_{CT} - K_{CTp}n_{CT}p + \mathcal{L}np - K_{cd}n_{CT} + G_{CTsp} = 0 \quad (2)$$

Here, n_{CT} is the charge transfer exciton density, τ_{CT} is the CT exciton lifetime, and K_{CTp} is the polaron-CT annihilation rate. The recombination of charges into CTs is taken to be an interfacial bimolecular Langevin process[30] with $\mathcal{L}$ being the Langevin rate coefficient. K_{cd} is the rate of CT exciton separating into free polarons where we use the Onsager−Braun formalism.[28] Note that by including both the Langevin recombination and the CT exciton dissociation, the model complies with the scheme suggested by Hilczer et al. as the source for effectively reduced Langevin recombination.[33] More on the validity of the Langevin and Onsager−Braun models can be found in the discussion section. G_{CTsp} is the thermal (spontaneous) generation of CT states. G_{CTsp} is derived in the Supporting Information by requiring equilibrium conditions to exist when there is no excitation (i.e., in the dark and under no bias). The equation for the holes is

$$\frac{dp}{dt} = \frac{J}{qa_0} + K_{cd}n_{CT} - \mathcal{L}np - N_T\frac{pn - n_{i,eff}^2}{\frac{1}{a}(n+\hat{n}) + \frac{1}{c}(p+\hat{p})} = 0 \quad (3)$$

Here, N_T is the density of deep states participating in the SRH process. a and c are capture cross section for electron or hole trap, respectively. As we consider the capture to be a bimolecular process, we use the known Langevin cross section $a = c = \mathcal{L} = \frac{q}{\varepsilon}(\mu_n + \mu_h)$, and the recombination is trap-assisted Langevin recombination.[3,4] $\hat{n} = n_{i,eff}\cdot\exp\left(\frac{E_T - E_{i,eff}}{k_bT}\right)$, $\hat{p} = n_{i,eff}\cdot\exp\left(\frac{E_{i,eff} - E_T}{k_bT}\right)$, where E_T is the trap level and $n_{i,eff}$ is the intrinsic charge density of the effective semiconductor made of the donor's HOMO and the acceptor's LUMO. $E_{i,eff}$ is the Fermi level that corresponds to $n_{i,eff}$.

A similar equation is written for the electrons (n) on the acceptor side of the junction. In the above, we equated 1−3 to zero as we will be interested in the steady state only.

To link between the applied bias, the current, and the polaron density, one needs to solve the drift diffusion equation on both sides of the junction using the charge densities at the junction and at the contacts as the boundary conditions (see the Supporting Information). If one assumes an equal voltage drop across the donor and acceptor sides, the resulting equations are

$$p = \underbrace{\left(p_c + \frac{Jd}{qV\mu_h}\right)\exp\left(-\frac{V}{2}\cdot\frac{\mu_h}{D_h}\right)}_{\text{diffusion}} \underbrace{-\frac{Jd}{qV\mu_h}}_{\text{drift term}} \quad (4)$$

$$n = \left(n_c + \frac{Jd}{qV\mu_n}\right)\exp\left(-\frac{V}{2}\cdot\frac{\mu_n}{D_n}\right) - \frac{Jd}{qV\mu_n} \quad (5)$$

where V is the built-in voltage (V_{bi}) minus the applied voltage (V_{app}), and d is the device length. Equations 1−5 constitute a full set that describes the planar heterojunction solar cell as a function of excitation density (G) and applied bias (V_{app}). p_c and n_c are, respectively, the positive polaron density on the donor side contact and the negative polaron density on the acceptor side contact:

$$p_c = N_{dos,HOMO,donor}\cdot\exp\left(-\frac{q\Delta_{anode,donor,HOMO}}{k_bT}\right) \quad (6)$$

$$n_c = N_{dos,LUMO,acceptor}\cdot\exp\left(-\frac{q\Delta_{cathode,acceptor,LUMO}}{k_bT}\right) \quad (7)$$

N_{DOS} is the density of states and Δ is the corresponding contact barrier for holes and electrons on the anode and cathode side, respectively.

As 1−3 are rate equations, where the processes are included explicitly, one could add or remove processes to represent different physical pictures of the junction. As we will show below, the above was the minimal set of processes required to reproduce the experimental data of both CuPc:C_{70}- and TAPC:C_{70}-based planar heterojunction devices. The symmetry we have assumed in deriving eqs 4 and 5 implies that we will be solving for one side only and consider the derived mobility as an effective one.

3. EXPERIMENTAL SECTION

3.1. Device Fabrication. All devices were fabricated on top of an indium tin oxide (ITO) coated glass substrate (PsiOTec Ltd.). The ITO substrates were covered by a patterned 100 nm polyimide layer, defining 18.4 mm^2 pixels and preventing leakage. The ITO substrates were cleaned and dried. The substrates were precleaned in an ultrasonic bath of acetone, methanol, and 2-propanol for 10 min each. They were then dried in a flow of nitrogen and further dried in an oven at 100 C for 60 min. Ultrahigh purity (UHP) grade organic materials copper phthalocyanine (CuPc), 4,4′-cyclohexylidenebis[*N*,*N*-bis(4-methylphenyl)benzenamine] (TAPC from Lumtec), was used as donors. UHP C70 fullerene (from CreaPhys) was used as acceptor, and a wide-energy-gap material 2,9-dimethyl-4,7-diphenyl-1,10-phenanthroline (Bathocuproine, or BCP, Sigma-Aldrich, purity 99.99%) was used as buffer material between the cathode and the active layer. Hole transport layer (HTL) was deposited by spin coating (poly(3,4-ethylenedioxythiophene):polystyrene sulfonic acid, Clevios PVP, Al 4083) PEDOT:PSS or copper thiocyanate (CuSCN, Sigma 99%), both 70 nm thick film. After the HTL was deposited, the substrates were dried in a flow of nitrogen and further dried in an oven at 100 °C for 60 min. CuPc (50 nm) or TAPC (50 nm), C70 (40 nm), and BCP (8 nm) and 30 nm thick Mg covered by a 60 nm thick Ag were thermally evaporated in a commercial vacuum deposition system (VINCI Technologies) at a base pressure of 6×10^7 mbar.

3.2. Measurement Procedures. Current−voltage characteristics were measured with a Keithley 2400 source meter. Spectrally resolved external quantum efficiency (EQE) was performed in the following way. Light from a tungsten halogen lamp (Oriel, 250 W QTH) was dispersed through a monochromator (Oriel, CS130). The light intensity was monitored using reference silicon and germanium photodetectors. Light from the monochromator (1.5 μW cm^{-2} at 600 nm) was chopped at 20 Hz, and the signal was read using a lock-in amplifier (EG&G 7265). Power-dependent quantum efficiency was measured using white light emitting diode metrics, whose intensity was controlled by the bias current. Appropriate optical density (OD) filters were used to extend the intensity range (~5 order) from ultralow to more than one

DOI: 10.1021/acs.jpcc.8b06404
J. Phys. Chem. C 2018, 122, 23271−23279

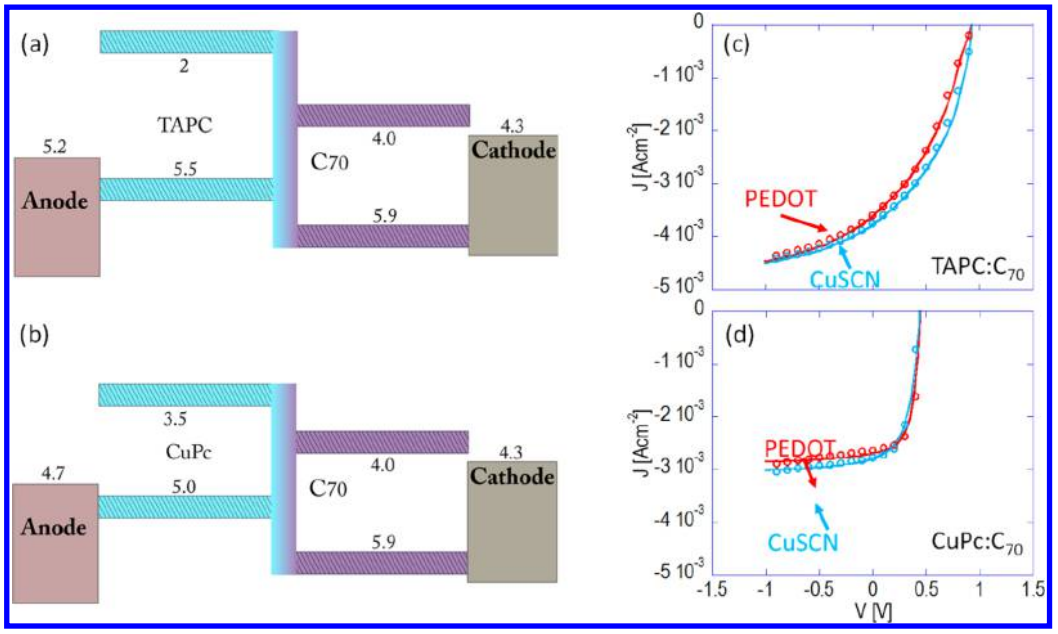

Figure 3. (a and b) Energy level diagram used as input parameters for the model where the contacts are taken to be within the gap. (a) TAPC:C_{70} device. (b) CuPc:C_{70} device. (c and d) Current density versus applied voltage under one sun. (c) For TAPC:C_{70} devices. (d) For CuPc:C_{70} devices. The circles are measured data, and the solid lines are model fits. The top (red) curves are for devices with PEDOT as the HTL, and the bottom (light blue) are for CuSCN as the HTL. In the case of PEDOT:TAPC:C_{70}, the presence of the slight S shape was found to be due to a slightly lower V_{bi}.

sun light intensity. Care was taken to ensure that the light spot falls within the pixel to avoid any potential edge effects. Measurement was done on several samples to ensure that the result is reproducible. Light intensity was monitored with a silicon photodetector, and the signal was read using a Keithley 2400 source meter.

4. RESULTS

Before presenting the series of measurements that have been conducted, we show in Figure 3a and b the energy level diagram used in the model for the TAPC:C_{70} and CuPc:C_{70} devices, respectively.[35−37] The injection contacts/layers are taken to be within the gap,[38,39] and the V_{OC} was used to fine-tune the cathode to anode energy difference (i.e., the built-in potential, V_{bi}). Other parameters that were taken as input constants are described in Table S1. Figure 3c and d shows an excellent fit of the model to the measured PCE curves of four different types of devices, different donors (TAPC and CuPC) and different HTLs (CuSCN and PEDOT). The PCE curve for PEDOT:TAPC:C_{70} shows a slight S shape, and indeed for this device the extracted built-in potential (V_{bi}) was 0.1 V lower as compared to the CuSCN device, resulting in $V_{bi} < V_{OC}$.

We chose to compare TAPC and CuPc devices as we are interested in examining the junction disorder role in a planar device. TAPC exhibits a relatively ordered junction, while the CuPC's junction exhibits high disorder. This difference is evident in the sub gap EQE of the junctions made with C70 (see Figure 4) where the CuPc:C_{70} devices show subgap response extending to lower energies.

The different measurement techniques used to deduce the TAPC device parameters, through fitting by the model, are shown in Figure 5. The left column is for the device structure of ITO:CuSCN:TAPC(50 nm):C_{70}(40 nm):BCP:Mg:Ag, and

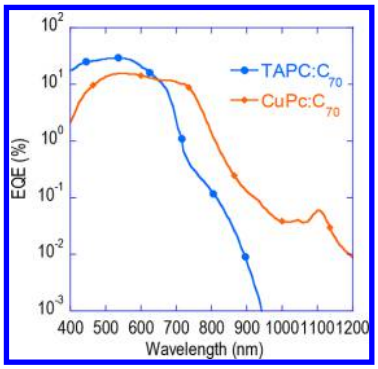

Figure 4. EQE as a function of excitation wavelength for CuPc:C_{70}- and TAPC:C_{70}-based devices.

the right column is for a device where PEDOT is replacing the CuSCN.

The first row, Figure 5a and b, shows the absolute value of the current density as a function of voltage for several light intensities. The dip in each curve is where the current changes sign and thus marks V_{OC}. This data set allows us to match the currents and make sure that the excitation dependence of the open circuit voltage is reproduced.

The second row, Figure 5c and d, shows the quantum efficiency (electrons per photons) as a function of light intensity and for several bias voltages. The low-intensity edge represents the free charge generation efficiency, and as the bias is changed it depicts the charge generation as a function of bias.[15,26,27,40] In the context of the processes shown in Figure 2, the charge generation efficiency at low intensity represents the path $[\text{exciton} \xrightarrow{K_{CT}} \text{charge-transfer exciton} \xrightarrow{K_{CD}} \text{charges}]$ with the rates as depicted above the arrows. As the excitation intensity increases, various loss mechanisms start to kick in.[15,41] As the relative weight of the loss mechanisms is also

DOI: 10.1021/acs.jpcc.8b06404
J. Phys. Chem. C 2018, 122, 23271−23279

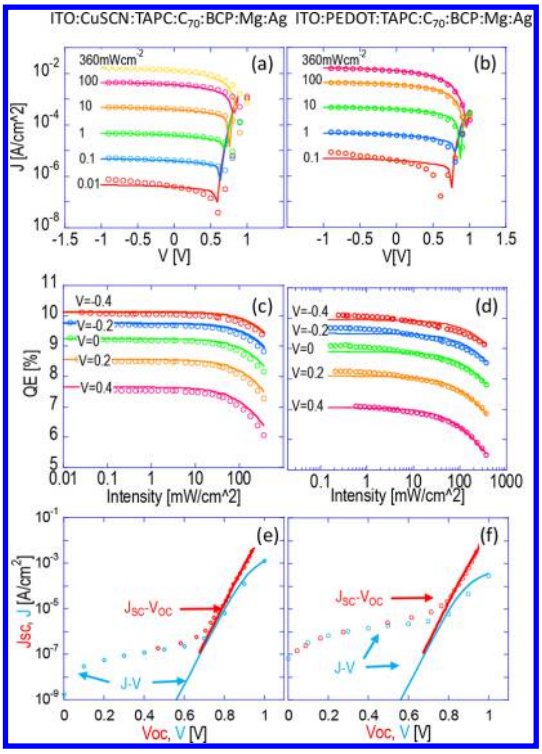

Figure 5. (a and b) Current density (absolute value) as a function of applied voltage and for several excitation intensities. (c and d) Quantum efficiency as a function of excitation intensity for several applied voltages. (e and f) Current density as a function of applied voltage under dark conditions (light blue ○) as well as short circuit current density versus open circuit voltage (red □) as was measured for a range of excitation intensities. Symbols, experiment; solid line, model fit.

bias dependent, it helps in quantifying the contribution of each.[27] For the charges we have two loss paths: [charges $\overset{\text{Langevin}}{\underset{K_{CD}}{\rightleftharpoons}}$ charge-transfer exciton] and [charges $\xleftrightarrow[\text{Trap assist. Lang. (SRH)}]{}$ deep-states]. When the device is optically excited, a process that reduces the charge generation manifests itself as a loss mechanism. In the current physical picture, such processes are the exciton-polaron annihilation[16] and CT-polaron annihilation with the rates K_{ep} and K_{CTp}, respectively. We remind the reader that in such annihilation process only the exciton or the CT exciton are annihilated while the charged polaron is not.

The third row, Figure 5e and f, contains two measurements. The first (in light blue) is the dark $J-V$, and the second (in red) is the short-circuit current (J_{SC}) as a function of the open circuit voltage (V_{OC}) as was measured for a range of excitation intensities.[11] The dark $J-V$ is composed of two parts: leakage current at low bias (<0.6 V) and diode behavior above 0.6 V. The slope of the diode's $J-V$, or the ideality factor, is governed only by charge recombination losses. This gives additional data, which help in separating the different loss mechanisms and confirm the observations from the QE measurement (second row). In addition, the absolute value of the dark $J-V$ allows one to deduce the effective mobility.

For the ideal diode, the photocurrent equals the dark current plus the short circuit current. Hence, the $J_{SC}-V_{OC}$ would be equal to the dark $J-V$. As Figure 5e and f shows, the planar heterojunction organic solar cell is not an ideal diode, and hence $J_{SC}-V_{OC} \neq J-V$. The fact that the model reproduces the diode part for both cases indicates that the difference between them is due to processes considered in Figure 2 and not due to parasitic effects, such as a shunt or serial resistance.[11] It is also interesting to note that the leakage part, which is not captured by the model, is almost identical between $J_{SC}-V_{OC}$ and $J-V$. This trend is inline with our recent publication suggesting that in these diodes the dark leakage current is associated with the junction and is not due to extrinsic effects.[42]

To reduce the number of fitted parameters, we assumed the donor (hole) and acceptor (electron) mobilities to be equal and used an effective mobility. While Figure 5 shows measurements results and model fittings for TAPC:C70 devices, Figure 6 shows the same but for CuPc being the donor in similar device structures.

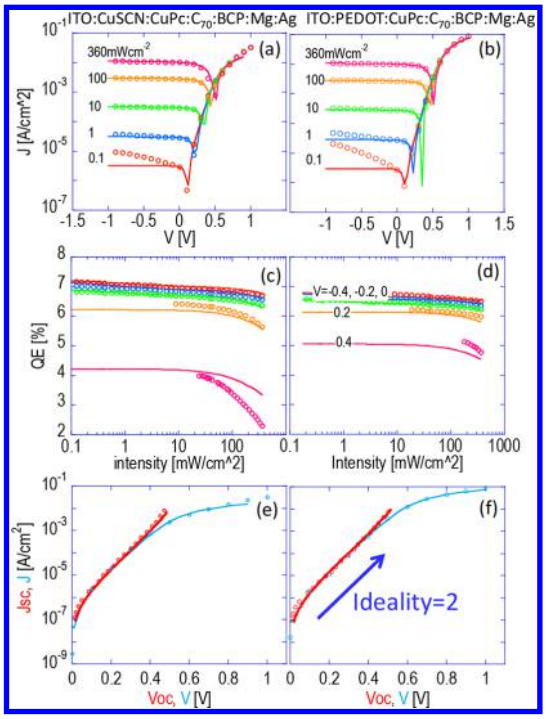

Figure 6. (a and b) Current density (absolute value) as a function of applied voltage and for several excitation intensities. (c and d) Quantum efficiency as a function of excitation intensity and for several applied voltages. (e and f) Current density as a function of applied voltage under dark conditions (light blue ○) as well as short circuit current density versus open circuit voltage (red □) as was measured for a range of excitation intensities. Symbols, experiment; solid line, model fit. The arrow in (f) depicts the slope that corresponds to a diode's ideality factor of 2.

Moving to the extracted parameters (Table 1), we note that the fitting and parameters extraction was carried out for both device structures (details of the fitting and extraction procedures can be found in the Supporting Information). We note that the significant difference between the use of PEDOT or CuSCN as the HTL was the built-in potential. The figures show another noticeable difference, which is the leakage current. However, the leakage current is outside the scope of this Article and is not described in the model.

5. DISCUSSION

A known effect of using bilayers is the low collection efficiency of the single junction, which reduces the charge generation rate

DOI: 10.1021/acs.jpcc.8b06404
J. Phys. Chem. C 2018, 122, 23271−23279

Table 1. Parameters Extracted through Fitting the Model to Experimental Data[a]

		PEDOT:CuPC:C70	CuSCN:CuPC:C70	PEDOT:TAPC:C70	CuSCN:TAPC:C70
effective mobility	$cm^2\ V^{-1}\ s^{-1}$	1.25×10^{-3}	1.25×10^{-3}	10^{-3}	10^{-3}
K_{ep}	$cm^{-3}\ s^{-1}$	2×10^{-8}	3×10^{-8}	10^{-8}	10^{-8}
$\hat{p}$	cm^{-3}	6×10^{12}	8×10^{12}	5.3×10^{16}	5.3×10^{16}
N_T	cm^{-3}	3×10^{16}	3×10^{16}	7×10^{16}	7×10^{16}
E_B	meV	20	20	74	74
V_{bi}	eV	0.49	0.4	0.83	0.94
K_{CT}	s^{-1}	2.61×10^{8}	2.81×10^{8}	5.1×10^{8}	5.1×10^{8}

[a]See Figures 5 and 6.

and the overall efficiency.[43] We recall that the low intensity limit of the QE versus intensity curves represents the charge generation efficiency.[27,41] Indeed, these curves (second row in Figure 5) show a relatively low charge generation efficiency (~10%), which is mainly attributed to the single junction. Nevertheless, we have chosen a bilayer structure as it is simpler to interpret with respect to the bulk heterojunction structure.

The model, or set of processes, shown in Figure 2 is the minimal set of processes we had to include to reproduce the set of measurements presented in Figures 5 and 6. Specifically, it was not sufficient to include only the forward and reverse reactions of charge generation and recombination through the CT state. It has been shown that accounting for the fact that a CT exciton, generated through charge recombination, can dissociate results in a reduced net recombination rate that could be orders of magnitude lower.[33] Using the diffusion limited reactions (Onsager−Braun, Langevin), we found that the net recombination losses were too low to reproduce the measured data. We arrived at this result through self-consistent fitting of the detailed model to the extensive data collected from the different measurement methods (see the Supporting Information). As the model framework is flexible, we added a charge recombination mechanism that enabled one to reproduce the measured data (the actual rates and the fitting procedure are detailed in the Supporting Information). Before discussing this extra loss mechanism, we note that having to add a charge recombination process means that the generation and recombination of charges do not necessarily proceed through the same set of states. This is a very positive conclusion as it indicates that through molecular and morphological design that eliminates the recombination path, the overall efficiency of organic solar cells can be significantly improved. This two-path picture is supported by existing literature as it is similar to stating that there are multiple interfacial bands of CT states[44] or that there are two pools of electron−hole pairs.[45] The above may also be considered as part of the discussions of the classic Langevin recombination model not describing well the recombination in disordered[46,47] and/or heterostructure devices.[10,14,30,48]

The loss mechanism we added is the trap-assisted recombination. For the CuPc devices, the ideality factor of the diode between 0.15 and 0.4 V is ~2 (Figure 6e,f), which is a common signature of trap-assisted recombination. Nevertheless, we note that adding trap-assisted recombination does not necessarily imply a monomolecular recombination. If the traps are shallow, and the device is operating in the trap-empty limit, then the trap-assisted recombination is bimolecular and the effect of including the traps is to enhance the bimolecular recombination. On the other hand, if the traps are deep such that they are always full, then the effect of the traps is to introduce a monomolecular recombination process. As discussed below, the above two scenarios are found in the ordered (TAPC:C_{70}) and disordered (CuPc:C_{70}) junctions.

For the TAPC:C_{70} device, we found that $\hat{p} = 5.3 \times 10^{16}$ cm^{-3}. Using the parameters in Table S1, this translates to trap energy being 0.25 eV into the gap. Because $\hat{p}$ is the charge density at which the traps are half-full, a value of 5.3×10^{16} cm^{-3} indicates that, under standard device operation, the traps are not full. The trap-assisted Langevin process is primarily bimolecular with the main effect being an enhancement of the bimolecular loss mechanism. For the CuPc:C_{70} device, however, we find that the traps are deep with $\hat{p} = 6 \times 10^{12}$ cm^{-3} and their position being 0.5 eV into the gap. This prediction of deep traps is a pure result of the fitting procedure; however, this agrees with the subgap EQE reported in Figure 4. Such low $\hat{p}$ implies that in the CuPc:C_{70} device the traps are full; this now introduces a monomolecular recombination process, and indeed the ideality factor of the dark $I-V$ (Figure 6e,f) is ~2 at low bias voltage. With the aid of the model and its being self-consistent, we could identify that there is more than one type of interface state with one mainly contributing to the charge generation and the other contributing to additional charge recombination losses. Also, the extracted energetic position of the extra states is in agreement with the amount of disorder observed in the subgap EQE (Figure 4).

In the suggested model (Figure 2), we propose a third loss mechanism, which is associated with charges (polarons) annihilating excitons before they may contribute to the charge generation process.[16,17,49,50] The relevant rates are K_{ep} and K_{CTp} for the exciton and CT (exciton), respectively. This process is well documented in the literature so there is no doubt that to some extent it is taking place.[51] The only question would be if it is significant or if there is any justification, given the set of measurements, to introduce a third mechanism. The extended set of measurements reported here allows us to answer this. The exciton-polaron annihilation loss differs from the already discussed loss mechanisms by the mere fact that it is not a charge-recombination process. As such, it has no effect on the charge generation-recombination processes taking place in the dark. Unlike the first two loss mechanisms, the exciton-polaron annihilation affects only the photoexcited properties (first two rows in Figures 5 and 6) but has no effect on the dark-current (third row in Figures 5 and 6). Although one could reproduce the dark characteristics, it is impossible to reproduce both the dark and the light characteristics without including the exciton-polaron annihilation process. However, out of the two possible exciton annihilations, the annihilation of CT by the polaron is not essential to the fit, which is reasonable, as in a bilayer the probability of a polaron to meet a CT on the surface of the single interface is orders of magnitude lower than the

DOI: 10.1021/acs.jpcc.8b06404
J. Phys. Chem. C 2018, 122, 23271−23279

probability of it to meet an exciton in the volume collected by the junction.

The last parameter to discuss is E_b. In the Onsager−Braun model,[28] dissociation of CTs into free polarons is proportional to the Langevin factor $\left(\mathcal{L} = \frac{q\langle\mu\rangle}{\langle\varepsilon\rangle\varepsilon_0}\right)$ times the factor $\exp\left(-\frac{E_b}{k_bT}\right)$. In the TAPC:$C_{70}$ device, the extracted E_b is close to 0.1 eV, which is on the low end of estimated CT binding energies.[52] For the CuPc:C_{70} device, the extracted binding energy is significantly lower. This is in agreement with the notion that the more disordered is the junction, the higher is the probability for CT exciton dissociation and charge generation.[19,52,53] One should note that stating that the binding energy includes effects such as entropy and disorder[19,52,53] is equivalent to saying that the Onsager−Braun model is not strictly valid,[54] and that, in this context, we actually use an effective binding energy.

To conclude, we presented a modeling framework, which is a useful tool to benchmark physical processes across devices and research laboratories. With this framework, one can reveal the relevant importance of various physical processes in OPVs and extract their parameters. The strength of this interpretation originates from the various measurement techniques in use and from the extensive data obtained, as one should remember that for a given set of measurements there is a limited number of processes that can be weighed independently. For example, without the dark characteristics, it would have been difficult to consider more than two loss mechanisms. This self-consistency forced us to suggest one set of sites (mainly) for charge generation and another (mainly) for charge recombination, leading to the conclusion that by careful treatment of the interface, it is possible to decrease the nonradiative (SRH) recombination and reach higher EQE and PCE. A similar conclusion is being reached in a very different system, as the perovskites, and the fact that generation and recombination do not proceed through the same states is common knowledge for silicon devices.

The strength of the set of measurement used lies in the fact that both bias and illumination conditions affect the balance of processes, that is, enhance one process while suppressing another. This is, for example, the reason for the differences in the plots of dark $J-V$ and of J_{sc} versus V_{oc}, differences that we were able to fit and justify through the model. It is also interesting to note that, despite the model's simplicity, it can reproduce fine details as the S shape (Figure 3c) or predict the traps energy and concentration.

As for expanding the model, we note that the model used assumes symmetry and does not distinguish between the n and p sides of the junction, and hence we stated that we discuss effective mobility and not μ_n and μ_p. We could afford that, because we were mainly interested in the processes taking place at the junction. Notably, when the dominant recombination is bimolecular, the effect of asymmetrical voltage drop on the donor and acceptor is negligible. In this case, carrier density dependence appears only in the form of the product of n and p, which is unaffected by the asymmetry. When the dominant recombination is monomolecular, the asymmetry may not be negligible, and an expanded mode is needed. To be able to independently deduce the parameters of both sides of the junction, one would need to introduce an additional set of measurements. The most obvious one would be to create a set of devices that differ only by the thickness of the n and p sides of the junction (the relevant equations are already in place).

■ ASSOCIATED CONTENT

Supporting Information

The Supporting Information is available free of charge on the ACS Publications website at DOI: 10.1021/acs.jpcc.8b06404.

Details of the dynamic drift diffusion device model (PDF)

■ AUTHOR INFORMATION

Corresponding Author

*E-mail: nir@technion.ac.il.

ORCID

Nir Tessler: 0000-0002-5354-3231

Notes

The authors declare no competing financial interest.

■ ACKNOWLEDGMENTS

This research was supported by the Israel Science Foundation (grant no. 488/16) and the Adelis Foundation for renewable energy research within the framework of the Grand Technion Energy Program (GTEP). H.S. acknowledges support by the Technion Ollendorff Minerva Center. Part of the device fabrication process was performed at the Technion's micro-nano fabrication & printing unit (MNF&PU).

■ REFERENCES

(1) NREL, National Renewable Energy Laboratory; https://www.nrel.gov/pv/assets/images/efficiency-chart.png (accessed May 12, 2018).

(2) Shockley, W.; Queisser, H. J. Detailed Balance Limit of Efficiency of P-N Junction Solar Cells. *J. Appl. Phys.* **1961**, *32*, 510−519.

(3) Janssen, R. A. J.; Nelson, J. Factors Limiting Device Efficiency in Organic Photovoltaics. *Adv. Mater.* **2013**, *25*, 1847−1858.

(4) Qin, Y.; Chen, Y.; Cui, Y.; Zhang, S.; Yao, H.; Huang, J.; Li, W.; Zheng, Z.; Hou, J. Achieving 12.8% Efficiency by Simultaneously Improving Open-Circuit Voltage and Short-Circuit Current Density in Tandem Organic Solar Cells. *Adv. Mater.* **2017**, *29*, 1606340−n/a.

(5) Wang, D.; Wright, M.; Elumalai, N. K.; Uddin, A. Stability of Perovskite Solar Cells. *Sol. Energy Mater. Sol. Cells* **2016**, *147*, 255−275.

(6) Liu, Y.; Zojer, K.; Lassen, B.; Kjelstrup-Hansen, J.; Rubahn, H.-G.; Madsen, M. Role of the Charge-Transfer State in Reduced Langevin Recombination in Organic Solar Cells: A Theoretical Study. *J. Phys. Chem. C* **2015**, *119*, 26588−26597.

(7) Koster, L. J. A.; Smits, E. C. P.; Mihailetchi, V. D.; Blom, P. W. M. Device Model for the Operation of Polymer/Fullerene Bulk Heterojunction Solar Cells. *Phys. Rev. B: Condens. Matter Mater. Phys.* **2005**, *72*, 085205.

(8) MacKenzie, R. C. I.; Kirchartz, T.; Dibb, G. F. A.; Nelson, J. Modeling Nongeminate Recombination in P3ht:Pcbm Solar Cells. *J. Phys. Chem. C* **2011**, *115*, 9806−9813.

(9) Blakesley, J. C.; Neher, D. Relationship between Energetic Disorder and Open-Circuit Voltage in Bulk Heterojunction Organic Solar Cells. *Phys. Rev. B: Condens. Matter Mater. Phys.* **2011**, *84*, 075210.

(10) Burke, T. M.; Sweetnam, S.; Vandewal, K.; McGehee, M. D. Beyond Langevin Recombination: How Equilibrium between Free Carriers and Charge Transfer States Determines the Open-Circuit Voltage of Organic Solar Cells. *Adv. Energy Mater.* **2015**, *5*, 1500123.

(11) Tvingstedt, K.; Deibel, C. Temperature Dependence of Ideality Factors in Organic Solar Cells and the Relation to Radiative Efficiency. *Adv. Energy Mater.* **2016**, *6*, 1502230.

DOI: 10.1021/acs.jpcc.8b06404
J. Phys. Chem. C 2018, 122, 23271−23279

(12) Hawks, S. A.; Li, G.; Yang, Y.; Street, R. A. Band Tail Recombination in Polymer:Fullerene Organic Solar Cells. *J. Appl. Phys.* **2014**, *116*, 074503.
(13) Kirchartz, T.; Nelson, J. Device Modelling of Organic Bulk Heterojunction Solar Cells. In *Multiscale Modelling of Organic and Hybrid Photovoltaics*; Beljonne, D., Cornil, J., Eds.; Springer-Verlag Berlin: Berlin, 2014; Vol. *352*, pp 279−324.
(14) Lakhwani, G.; Rao, A.; Friend, R. H. Bimolecular Recombination in Organic Photovoltaics. *Annu. Rev. Phys. Chem.* **2014**, *65*, 557−581.
(15) Tzabari, L.; Wang, J.; Lee, Y.-J.; Hsu, J. W. P.; Tessler, N. Role of Charge Transfer States in P3ht-Fullerene Solar Cells. *J. Phys. Chem. C* **2014**, *118*, 27681−27689.
(16) Tzabari, L.; Zayats, V.; Tessler, N. Exciton Annihilation as Bimolecular Loss in Organic Solar Cells. *J. Appl. Phys.* **2013**, *114*, 154514.
(17) Szmytkowski, J. Nongeminate Recombination in Organic Bulk Heterojunction Solar Cells: Contribution of Exciton−Polaron Interaction. *Phys. Status Solidi RRL* **2012**, *6*, 300−302.
(18) Proctor, C. M.; Kuik, M.; Nguyen, T.-Q. Charge Carrier Recombination in Organic Solar Cells. *Prog. Polym. Sci.* **2013**, *38*, 1941−1960.
(19) Clarke, T. M.; Durrant, J. R. Charge Photogeneration in Organic Solar Cells. *Chem. Rev.* **2010**, *110*, 6736−6767.
(20) Zhou, Y.; Long, G.; Li, A.; Gray-Weale, A.; Chen, Y.; Yan, T. Towards Predicting Power Conversion Efficiencies of Organic Solar Cells from Donor and Acceptor Molecule Structures. *J. Mater. Chem. C* **2018**, *6*, 3276.
(21) Liu, B.; Png, R.-Q.; Tan, J.-K.; Ho, P. K. H. Evaluation of Built-in Potential and Loss Mechanisms at Contacts in Organic Solar Cells: Device Model Parameterization, Validation, and Prediction. *Adv. Energy Mater.* **2014**, *4*, 1200972.
(22) Cheyns, D.; Poortmans, J.; Heremans, P.; Deibel, C.; Verlaak, S.; Rand, B. P.; Genoe, J. Analytical Model for the Open-Circuit Voltage and Its Associated Resistance in Organic Planar Heterojunction Solar Cells. *Phys. Rev. B: Condens. Matter Mater. Phys.* **2008**, *77*, 165332.
(23) Nakano, K.; Tajima, K. Organic Planar Heterojunctions: From Models for Interfaces in Bulk Heterojunctions to High-Performance Solar Cells. *Adv. Mater.* **2017**, *29*, 1603269−n/a.
(24) Giebink, N. C.; Wiederrecht, G. P.; Wasielewski, M. R.; Forrest, S. R. Ideal Diode Equation for Organic Heterojunctions. I. Derivation and Application. *Phys. Rev. B: Condens. Matter Mater. Phys.* **2010**, *82*, 12.
(25) Griffith, O. L.; Liu, X.; Amonoo, J. A.; Djurovich, P. I.; Thompson, M. E.; Green, P. F.; Forrest, S. R. Charge Transport and Exciton Dissociation in Organic Solar Cells Consisting of Dipolar Donors Mixed with C70. *Phys. Rev. B: Condens. Matter Mater. Phys.* **2015**, *92*, 085404.
(26) Shekhar, H.; Tzabari, L.; Solomeshch, O.; Tessler, N. Thickness Dependent Charge Transfer States and Dark Carriers Density in Vacuum Deposited Small Molecule Organic Photocell. *J. Appl. Phys.* **2016**, *120*, 155501.
(27) Tzabari, L.; Wang, J.; Lee, Y.-J.; Hsu, J. W. P.; Tessler, N. Role of Contact Injection, Exciton Dissociation, and Recombination, Revealed through Voltage and Intensity Mapping of the Quantum Efficiency of Polymer:Fullerene Solar Cells. *J. Phys. Chem. C* **2016**, *120*, 10146−10155.
(28) Braun, C. L. Electric Field Assisted Dissociation of Charge Transfer States as a Mechanism of Photocarrier Production. *J. Chem. Phys.* **1984**, *80*, 4157−4161.
(29) Ferguson, A. J.; Kopidakis, N.; Shaheen, S. E.; Rumbles, G. Dark Carriers, Trapping, and Activation Control of Carrier Recombination in Neat P3ht and P3ht:Pcbm Blends. *J. Phys. Chem. C* **2011**, *115*, 23134−23148.
(30) Koster, L. J. A.; Mihailetchi, V. D.; Blom, P. W. M. Bimolecular Recombination in Polymer/Fullerene Bulk Heterojunction Solar Cells. *Appl. Phys. Lett.* **2006**, *88*, 052104.
(31) Shockley, W.; Read, W. T. Statistics of the Recombinations of Holes and Electrons. *Phys. Rev.* **1952**, *87*, 835−842.
(32) Hall, R. N. Electron-Hole Recombination in Germanium. *Phys. Rev.* **1952**, *87*, 387.
(33) Hilczer, M.; Tachiya, M. Unified Theory of Geminate and Bulk Electron-Hole Recombination in Organic Solar Cells. *J. Phys. Chem. C* **2010**, *114*, 6808−6813.
(34) Wetzelaer, G. A. H.; Kuik, M.; Nicolai, H. T.; Blom, P. W. M. Trap-Assisted and Langevin-Type Recombination in Organic Light-Emitting Diodes. *Phys. Rev. B: Condens. Matter Mater. Phys.* **2011**, *83*, 5.
(35) Chassé, T.; Wu, C. I.; Hill, I.; Kahn, A. Band Alignment at Organic-Inorganic Semiconductor Interfaces: A-Npd and Cupc on Inp(110). *J. Appl. Phys.* **1999**, *85*, 6589−6592.
(36) Cui, L.-S.; Liu, Y.; Yuan, X.-D.; Li, Q.; Jiang, Z.-Q.; Liao, L.-S. Bipolar Host Materials for High Efficiency Phosphorescent Organic Light Emitting Diodes: Tuning the Homo/Lumo Levels without Reducing the Triplet Energy in a Linear System. *J. Mater. Chem. C* **2013**, *1*, 8177−8185.
(37) Wang, Z.; Yokoyama, D.; Wang, X.-F.; Hong, Z.; Yang, Y.; Kido, J. Highly Efficient Organic P-I-N Photovoltaic Cells Based on Tetraphenyldibenzoperiflanthene and Fullerene C70. *Energy Environ. Sci.* **2013**, *6*, 249−255.
(38) Braun, S.; Salaneck, W. R.; Fahlman, M. Energy-Level Alignment at Organic/Metal and Organic/Organic Interfaces. *Adv. Mater.* **2009**, *21*, 1450−1472.
(39) Magen, O.; Tessler, N. On Electrode Pinning and Charge Blocking Layers in Organic Solar Cells. *J. Appl. Phys.* **2017**, *121*, 195502.
(40) Tzabari, L.; Tessler, N. Shockley–Read–Hall Recombination in P3ht:Pcbm Solar Cells as Observed under Ultralow Light Intensities. *J. Appl. Phys.* **2011**, *109*, 064501.
(41) Rappaport, N.; Solomesch, O.; Tessler, N. The Interplay between Space Charge and Recombination in Conjugated Polymer/Molecule Photocells. *J. Appl. Phys.* **2005**, *98*, 033714.
(42) Shekhar, H.; Solomeshch, O.; Liraz, D.; Tessler, N. Low Dark Leakage Current in Organic Planar Heterojunction Photodiodes. *Appl. Phys. Lett.* **2017**, *111*, 223301.
(43) Forrest, S. R. The Limits to Organic Photovoltaic Cell Efficiency. *MRS Bull.* **2005**, *30*, 28−32.
(44) Ndjawa, G. O. N.; Graham, K. R.; Mollinger, S.; Wu, D. M.; Hanifi, D.; Prasanna, R.; Rose, B. D.; Dey, S.; Yu, L.; Bredas, J.; McGehee, M. D.; Salleo, A.; Ammassian, A. Open-Circuit Voltage in Organic Solar Cells: The Impacts of Donor Semicrystallinity and Coexistence of Multiple Interfacial Charge-Transfer Bands. *Adv. Energy Mater.* **2017**, *7*, 1601995.
(45) Causa, M.; De Jonghe-Risse, J.; Scarongella, M.; Brauer, J. C.; Buchaca-Domingo, E.; Moser, J.-E.; Stingelin, N.; Banerji, N. The Fate of Electron−Hole Pairs in Polymer:Fullerene Blends for Organic Photovoltaics. *Nat. Commun.* **2016**, *7*, 12556.
(46) Adriaenssens, G. J.; Arkhipov, V. I. Non-Langevin Recombination in Disordered Materials with Random Potential Distributions. *Solid State Commun.* **1997**, *103*, 541−543.
(47) Preezant, Y.; Tessler, N. Exciton Formation as a Rate Limiting Step for Charge Recombination in Disordered Organic Molecules or Polymers. *J. Appl. Phys.* **2011**, *109*, 013701.
(48) Shoaee, S.; Stolterfoht, M.; Neher, D. The Role of Mobility on Charge Generation, Recombination, and Extraction in Polymer-Based Solar Cells. *Adv. Energy Mater.* **2018**, *0*, 1703355.
(49) Szmytkowski, J. Four-Body Recombination in Organic Bulk Heterojunction Solar Cells: An Alternative Interpretation. *Semicond. Sci. Technol.* **2013**, *28*, 052002.
(50) Głowienka, D.; Szmytkowski, J. Influence of Excitons Interaction with Charge Carriers on Photovoltaic Parameters in Organic Solar Cells. *Chem. Phys.* **2018**, *503*, 31−38.
(51) Pope, M.; Swenberg, C. E. *Electronic Processes in Organic Crystals*; Clarendon Press: Oxford, 1982.

DOI: 10.1021/acs.jpcc.8b06404
J. Phys. Chem. C 2018, 122, 23271−23279

(52) van Eersel, H.; Janssen, R. A. J.; Kemerink, M. Mechanism for Efficient Photoinduced Charge Separation at Disordered Organic Heterointerfaces. *Adv. Funct. Mater.* **2012**, *22*, 2700−2708.
(53) Hood, S. N.; Kassal, I. Entropy and Disorder Enable Charge Separation in Organic Solar Cells. *J. Phys. Chem. Lett.* **2016**, *7*, 4495−4500.
(54) Albrecht, U.; Bassler, H. Efficiency of Charge Recombination in Organic Light Emitting Diodes. *Chem. Phys.* **1995**, *199*, 207−214.

DOI: 10.1021/acs.jpcc.8b06404
J. Phys. Chem. C 2018, 122, 23271−23279